*Article*

# A Rare Natural Benzo[*k*,*l*]xanthene as a Turn-Off Fluorescent Sensor for Cu$^{2+}$ Ion

**Giuseppe Floresta** [1] , **Nunzio Cardullo** [2,\*] , **Carmela Spatafora** [2,†] , **Antonio Rescifina** [1,\*] and **Corrado Tringali** [2]

1    Department of Drug Sciences, University of Catania, Viale A. Doria 6, 95125 Catania, Italy;
     giuseppe.floresta@unict.it
2    Department of Chemical Sciences, University of Catania, Viale A. Doria 6, 95125 Catania, Italy;
     cspatafo@unict.it (C.S.); ctringali@unict.it (C.T.)
\*    Correspondence: ncardullo@unict.it (N.C.); arescifina@unict.it (A.R.)
†    Dedicated to Professor Carmela Spatafora, a friend, colleague, and distinguished scientist, who prematurely
     passed away during the preparation of the paper.

check for
updates

**Abstract:** Rapid and efficient analyses of copper ions are crucial to providing key information for Cu$^{2+}$ in living cells because of their biological importance. In this study, we reported one new turn-off fluorescent sensor for Cu$^{2+}$ with a benzo[*k*,*l*]xanthene core, which served as an efficient cation sensor for copper ion over a wide range of other cations (Na$^+$, K$^+$, Ag$^+$, Hg$^{2+}$, Cd$^{2+}$, Co$^{2+}$, Ni$^{2+}$, Zn$^{2+}$, Mg$^{2+}$, and Fe$^{3+}$) owing to the catechol group in the aromatic core. The sensor showed selectivity for Cu$^{2+}$ over other ions; the log$K_\beta$ for Cu$^{2+}$ binding to compound **1** had a value of 13.265. In the presence of Cu$^{2+}$, sensor **1** provided significant fluorescence decrement; Co$^{2+}$, and Ni$^{2+}$ caused a fluorescence decrement when employed at a higher concentration than Cu$^{2+}$, while Na$^+$, K$^+$, Hg$^{2+}$, Cd$^{2+}$, Zn$^{2+}$, and Mg$^{2+}$ metal ions produced only minor changes in fluorescence intensity. Fluorescence experiments demonstrate that compound **1** may have an application as a fluorescent probe for detecting Cu$^{2+}$ with a limit of detection of 0.574 μM.

**Keywords:** polyphenols; lignans; fluorescent sensor; natural-derived ligand

## 1. Introduction

The design and synthesis of fluorescent sensors with high selectivity for cations have recently received considerable attention because of the fundamental role of cations in living systems. Indeed, some ions such as sodium, potassium, magnesium, and calcium are involved in many biological processes, and the effective control of their levels is of fundamental importance in medicine.

The development of sensitive and effective fluorescent sensors for heavy transition metal ions is also of current interest. These metals are used in many different industrial processes, and there is a high risk of their release into the environment; consequently, the search for methods to monitor and reveal these ions is of great relevance.

Among the various ions of this type, copper is worth particular attention; in fact, it has a catalytic role as a cofactor for a variety of metalloenzymes, including superoxide dismutase, cytochrome c, oxidase, and tyrosinase. However, in conditions that favor accumulation, copper can cause neurodegenerative diseases [1] (there is evidence regarding, for example, Alzheimer's disease and Wilson's disease), probably because of its involvement in the production of reactive oxygen species [2]. Because of its biological importance, fluorescent chemosensors that are able to monitor Cu$^{2+}$ in living cells have attracted much attention in recent years [3–8].

Due to its high sensitivity and selectivity, as well as its noninvasive nature, fluorescence is very often selected as a signal for chemical sensing events.

Lately, our group has been involved in the synthesis, mediated by metals or enzymes, of bioinspired lignans and neolignans, including dimeric caffeic acid derivatives [9–16]. Notably, the oxidative coupling, mediated by manganese acetate (III), of caffeic acid esters or amides allowed us to obtain some natural and unnatural lignans with a planar and intensively fluorescent benzo[*k,l*]xanthene core, very rarely found in nature, exemplified by compound **1** (Figure 1) [17], which has recently been isolated from *Orobanche cernua* Loefling [18].
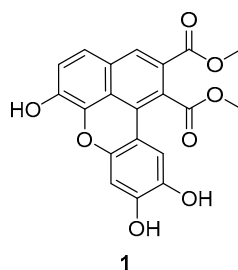


**1**

**Figure 1.** Structure of compound **1**.

Because of the rarity of benzoxanthene lignans, their biological properties and possible applications are almost unexplored if we exclude some works in which these compounds have been proven as antifungal agents [19], anti-inflammatory agents [20], and useful antiproliferative compounds against different tumor cell lines, with antioxidant and antiangiogenic activities [17,21–23]. Some of these compounds were also subjected to STD-NMR measurements and molecular docking calculations; the obtained data indicate that benzoxanthene lignans interact with the DNA in two ways: the planar core intercalates between two base pairs in the DNA while the ester groups, which behave as flexible pendants, bind to the minor groove of the nucleic acid [17]. Moreover, the benzoxanthene lignans are strongly fluorescent both in solution and in the solid-state under UV-light at 366 nm, and this property may be of high interest for the design of new fluorescent probes for biomedical applications.

In this study, we investigated if the natural product **1**, selected among different previously reported compounds with a benzo[*k,l*]xanthene core, may be able to recognize metal cations that are involved in biological systems or that accumulate in the environment, namely $Ag^+$, $Cd^{2+}$, $Co^{2+}$, $Cu^{2+}$, $Fe^{3+}$, $Hg^{2+}$, $K^+$, $Mg^{2+}$, $Na^+$, $Ni^{2+}$, and $Zn^{2+}$ [24,25].

## 2. Results and Discussion

The naturally occurring benzoxanthene lignan **1** was synthesized according to a biomimetic methodology based on the oxidative coupling of methyl caffeate, as previously reported [17]. The details are given in the experimental section.

The binding ability of compound **1** toward different metal cations ($Na^+$, $K^+$, $Ag^+$, $Hg^{2+}$, $Cd^{2+}$, $Co^{2+}$, $Ni^{2+}$, $Zn^{2+}$, $Mg^{2+}$, $Cu^{2+}$, and $Fe^{3+}$) was studied by employing UV-Vis spectroscopy and fluorescence experiments. The progressive quenching of the fluorescence and any possible displacements of the absorption maxima in the UV-Vis spectrum were monitored as an indication of a structural variation of the substrate due to the interaction with the metal ion [26].

In Figure 2, we report the UV and fluorescence spectra ($\lambda$ excitation at 366 nm) of compound **1** ($1.72 \times 10^{-5}$ M) in an ethanol-phosphate buffer (1:1).
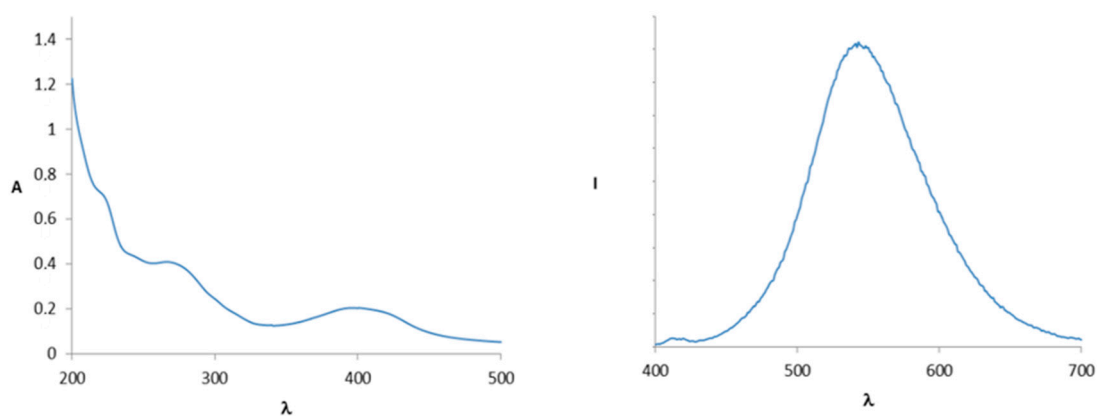
**Figure 2.** UV spectrum (**left**) and fluorescence spectrum (**right**) (excitation at 366 nm) of compound **1** ($c = 1.72 \times 10^{-5}$ M).

Subsequently, a series of solutions ($10^{-2}$ M) of monovalent, bivalent, and trivalent ions, namely $Na^+$, $K^+$, $Ag^+$, $Hg^{2+}$, $Cd^{2+}$, $Co^{2+}$, $Ni^{2+}$, $Zn^{2+}$, $Mg^{2+}$, $Cu^{2+}$, and $Fe^{3+}$, were prepared. The solutions were then used to record the UV and fluorescence spectra (Figures 3–7) by successive additions of 10 μL aliquots to a solution of compound **1** in an ethanol-phosphate buffer 1:1 mixture ($c = 1.72 \times 10^{-5}$ M).
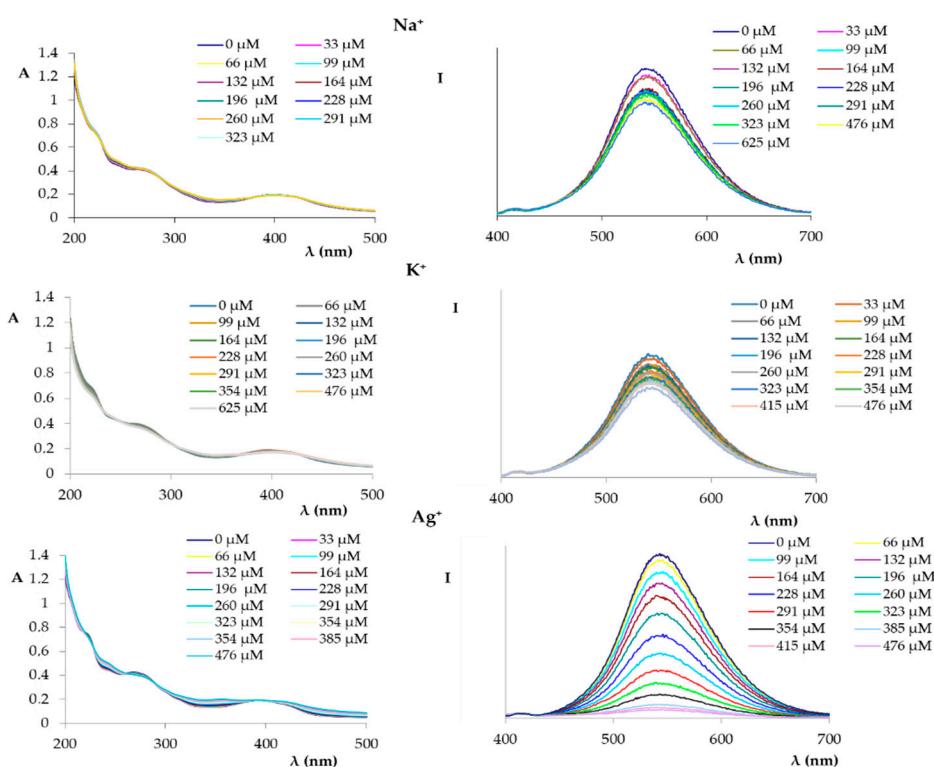


**Figure 3.** UV spectra (**left**) and fluorescence spectra (**right**) (excitation at 366 nm) of compound **1** ($1.72 \times 10^{-5}$ M in EtOH:phosphate buffer) titrated with an increasing amount of monovalent cations ($1.0 \times 10^{-2}$ M in phosphate buffer).
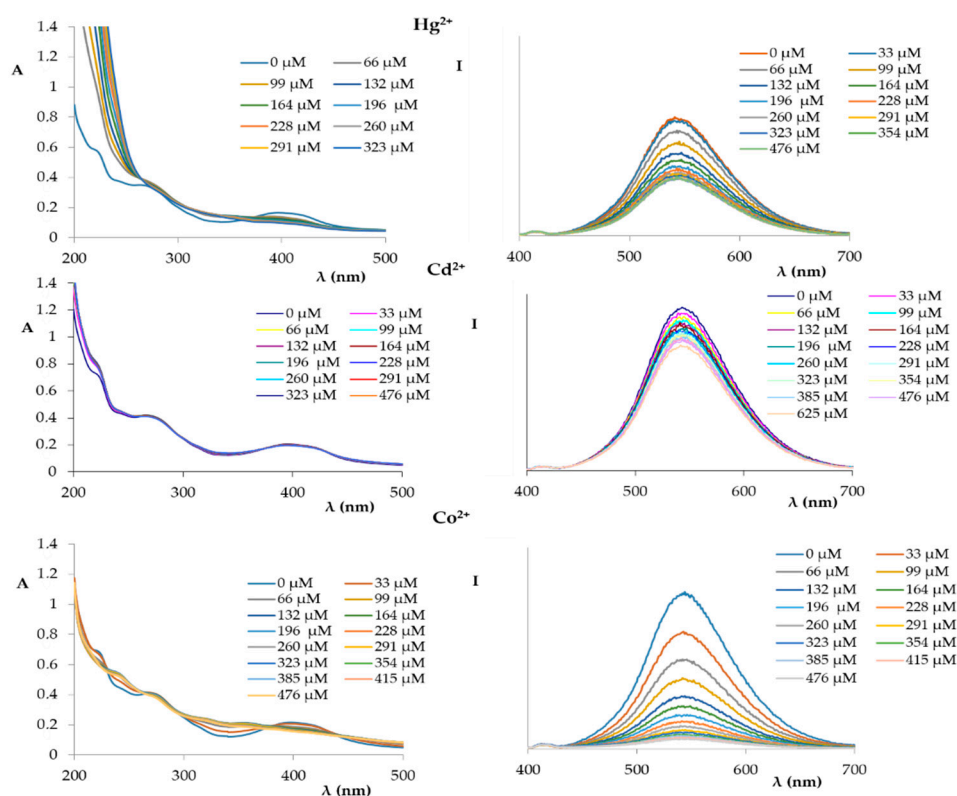
**Figure 4.** UV spectra (**left**) and fluorescence spectra (**right**) (excitation at 366 nm) of compound **1** ($1.72 \times 10^{-5}$ M in EtOH:phosphate buffer) titrated with an increasing amount of $Hg^{2+}$, $Cd^{2+}$, and $Co^{2+}$ ($1.0 \times 10^{-2}$ M in phosphate buffer).

Figure 3 shows the UV and fluorescence spectra recorded in the presence of an increasing amount of the studied monovalent cations ($Na^+$, $K^+$, and $Ag^+$).

As shown in Figure 3, the UV spectra did not show significant changes in the maxima absorption when compound **1** was titrated with each of the cations. However, some changes were observed in the fluorescence spectra. Notably, the spectra recorded in the presence of $Na^+$ and $K^+$ ions showed a maximum variation of 20 units initially, and subsequently, while increasing the concentration of the metal ions, no changes were observed. A different trend was observed when the same titration was carried out with $Ag^+$ ions; in fact, a progressive decrease of the fluorescence intensity during the whole $Ag^+$ titration was observed, which indicates an interaction between compound **1** and the $Ag^+$ ions.

Both the UV and fluorescence spectra of compound **1** recorded in the presence of increasing amounts of divalent cations ($Hg^{2+}$, $Cd^{2+}$, $Co^{2+}$, $Ni^{2+}$, $Zn^{2+}$, $Mg^{2+}$, $Cu^{2+}$) are shown in Figures 4 and 5.

The spectra acquired by titration of compound **1** with $Cd^{2+}$, $Hg^{2+}$, $Zn^{2+}$, and $Mg^{2+}$ showed only an initial decrease of the fluorescence signal that subsequently reached a plateau, similar to the sodium and potassium ions.

However, a different trend was observed when the titration was made with $Co^{2+}$ and $Ni^{2+}$. In these cases, a progressive decrease in the intensity of the measured fluorescence was measured, similar to the silver ion.

A completely different trend was observed for the titration of the solution of compound **1** with a $1.0 \times 10^{-2}$ M $Cu^{2+}$ ion solution (Figure 5); in fact, the fluorescence was completely switched off after the first addition (10 μL) of the copper solution.

Therefore, further measures were carried out by lowering the concentration of $Cu^{2+}$ ions. In Figure 6, the curves of the fluorimetric titrations of a solution of compound **1** ($1.72 \times 10^{-5}$ M) with increasing amounts of a solution of copper nitrate ($1.0 \times 10^{-3}$ M and $1.0 \times 10^{-4}$ M) are shown. As can

be observed, increasing the copper concentration via additions of a $10^{-4}$ M $Cu^{2+}$ solution caused a linear reduction in the fluorescence intensity of the probe.

Figure 7 shows the UV and fluorescence spectra of compound **1** recorded in the presence of increasing amounts of $Fe^{3+}$. Similar to what was observed for $Ag^{2+}$, a progressive decrease in the intensity of the fluorescence of compound **1** was observed as a result of increasing additions of ferric ion.

The fluorescence of the benzoxanthene **1** in the presence of different metal ions was initially studied in the stoichiometric ratio of 1:1. From this study, it is evident that the intensity of fluorescence decreases after the addition of the different metal ions, and the extent of quenching depends on the different capacities of the metal ions to bind with the ligand. The addition of the studied metal ions other than $Ag^+$, $Cu^{2+}$, and $Fe^{3+}$ only produced a minimal change in the intensity of emission at 543 nm.
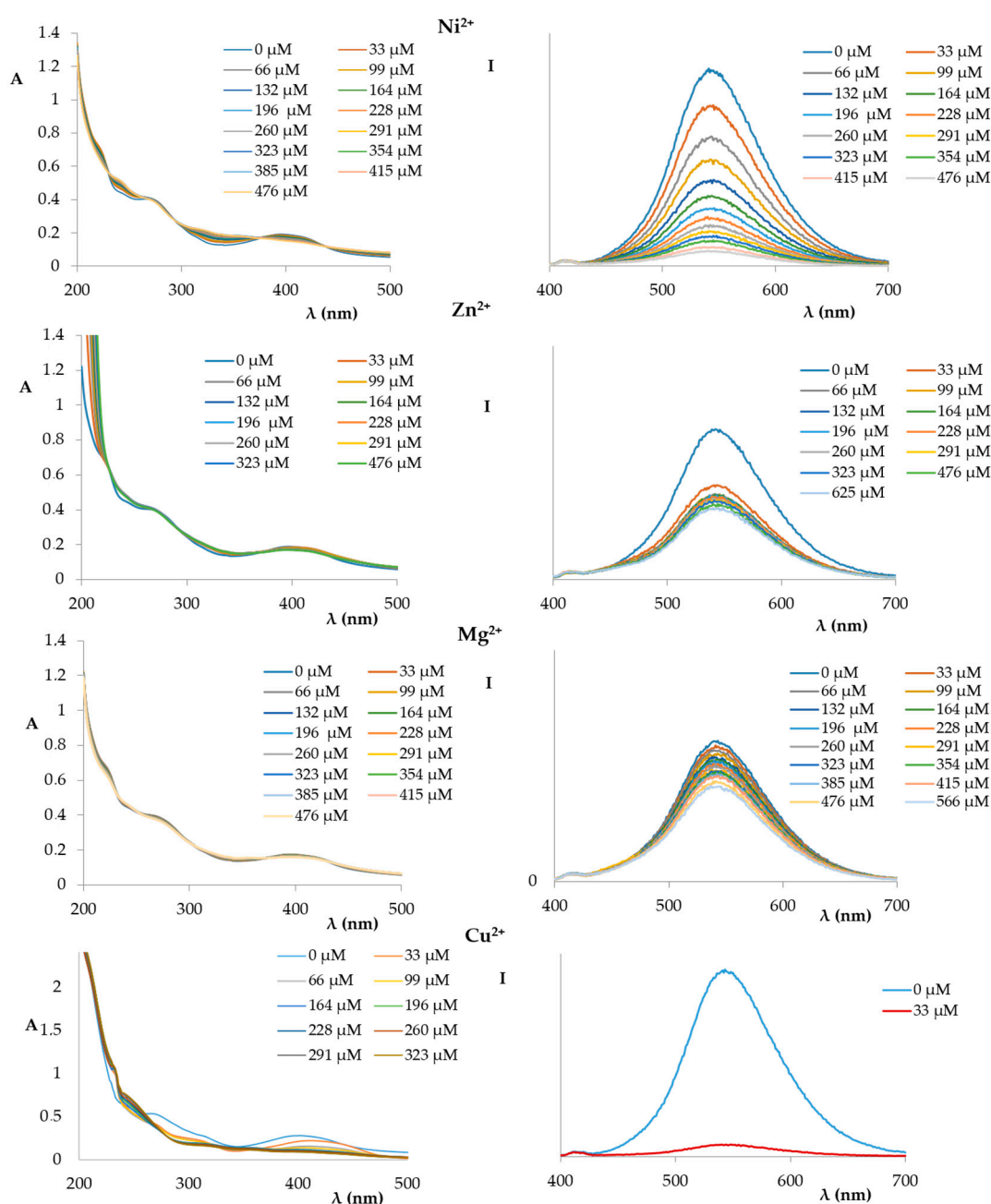


**Figure 5.** UV spectra (**left**) and fluorescence spectra (**right**) (excitation at 366 nm) of compound **1** ($1.72 \times 10^{-5}$ M in EtOH:phosphate buffer) titrated with an increasing amount of $Ni^{2+}$, $Zn^{2+}$, $Mg^{2+}$, and $Cu^{2+}$ ($1.0 \times 10^{-2}$ M in phosphate buffer).
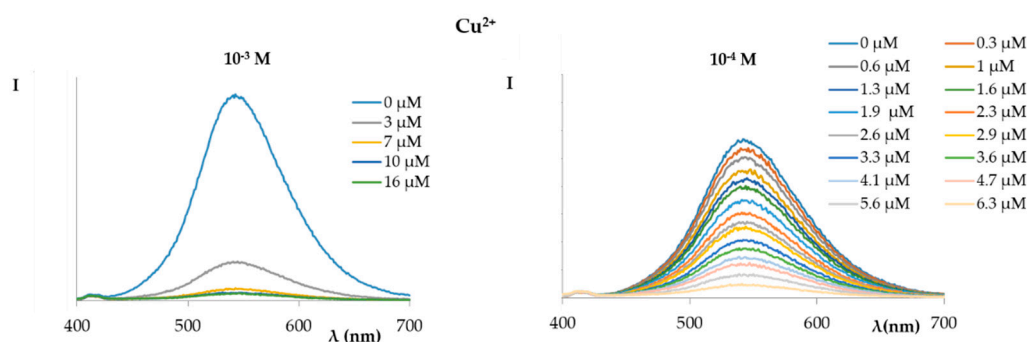
**Cu²⁺**



**Figure 6.** Fluorescence (excitation at 366 nm) spectra of compound **1** ($1.72 \times 10^{-5}$ M in EtOH:phosphate buffer) titrated with increasing amounts of a copper nitrate solution ((**left**) $1.0 \times 10^{-3}$ M; (**right**) $1.0 \times 10^{-4}$ M).
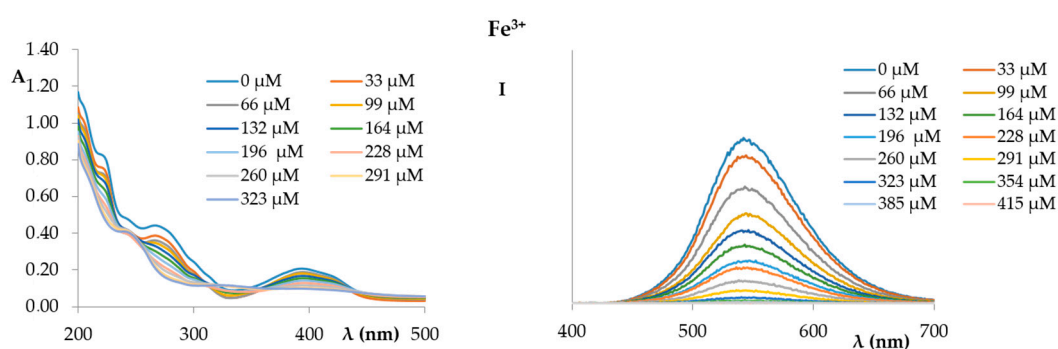
**Fe³⁺**



**Figure 7.** UV spectra (**left**) and fluorescence spectra (**right**) (excitation at 366 nm) of compound **1** ($1.72 \times 10^{-5}$ M in EtOH:phosphate buffer) titrated with an increasing amount of $Fe^{3+}$ ($1.0 \times 10^{-2}$ M in phosphate buffer).

Figure 8 shows the ratio of fluorescence quenching for the different examined ions, calculated as $(I_0 - I)/I_0$, which shows that $Cu^{2+}$ led to a complete fluorescence quenching (98.7%), followed by $Ag^+$ (82%) and $Fe^{3+}$ (57%). Moreover, the natural probe **1** responded with high selectivity toward $Cu^{2+}$ over the other metal ions, as confirmed by competing experiments (Figure 8, left). The fluorescence measurements of mixtures containing compound **1** in the presence of $Cu^{2+}$ (1.4 μM) and one of the other metal ions ($Na^+$, $K^+$, $Zn^{2+}$, $Cd^{2+}$, $Co^{2+}$, $Ni^{2+}$, $Hg^{2+}$, and $Mg^{2+}$; each 40 μM) showed no relevant interference effect on the interaction of the Cu ion with the probe, even when the other cation was present in solution at a 30-fold higher concentration. Conversely, the experiments performed in the same conditions with $Fe^{3+}$ and with $Ag^+$ demonstrated a lower selectivity of probe **1** towards Cu ions, mostly in the presence of Ag ions.

Due to the high selectivity for $Cu^{2+}$ and $Ag^+$, subsequent studies were conducted only for these two ions.

The subsequent step was a study aimed at determining the stoichiometric ratio of metal–ligand and the binding affinities between the $Cu^{2+}$ and $Ag^+$ ions and compound **1**.

The association constants of the complexes ($Cu^{2+}$/compound **1** and $Ag^+$/compound **1**) were determined using UV and fluorescence titrations in solution followed by non-linear least-square regression. The titrations were also used to determine the stoichiometry of the obtained inclusion complexes. Different stoichiometries were tested (1:1, 1:2, 1:3; metals:compound **1**). The general method relying on the analysis of residual distribution in titration data fitting, considered the most reliable for establishing a proper binding model, was applied. After the refinement, the residuals with the 1:2 model for the $Ag^+$ and the 1:3 model for the $Cu^{2+}$ did not show a systematical trend, indicating that no relevant concentration of other complexes was formed under these experimental conditions. The association constant ($K_\beta$) was evaluated when the concentration of compound **1** was fixed and the

concentration of the metal was varied, as described in the experimental section. In the case of silver, the $\log K_\beta$ resulted in 6.589 ± 0.005, while for copper, we obtained a value of 13.265 ± 0.025, confirming the high selectivity of compound **1** for $Cu^{2+}$.
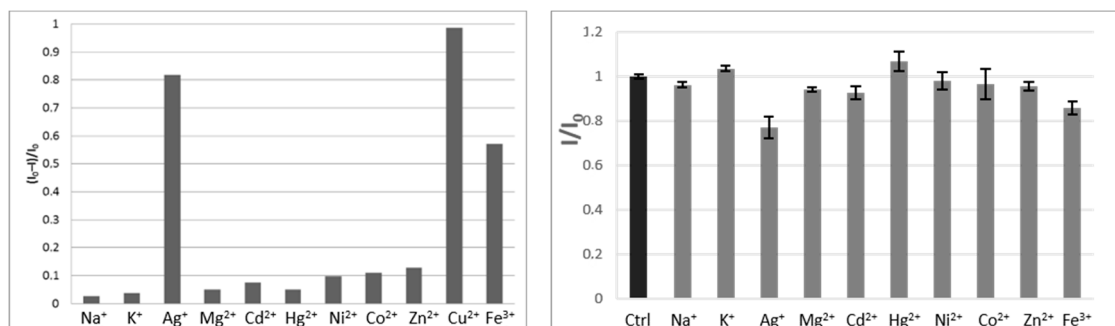


**Figure 8.** (**Left**) Comparison of the fluorescence intensity of compound **1** ($1.72 \times 10^{-5}$ M) with the studied metal ions (30 μM). (**Right**) Selectivity of compound **1** towards the studied cations. The concentration of $Cu^{2+}$ was 1.4 μM; the concentration of the other metal ions was 40 μM. $I_0$ and $I$ are the fluorescence intensities of the mixtures of compound **1** and $Cu^{2+}$ ions in the absence (Ctrl) and presence of other metals, respectively. Error bars represent standard deviations, as means of three experiments.

Furthermore, based on this data, the fluorescence quenching process for probe **1** in the presence of copper ions was studied by the Stern–Volmer Equation [27],

$$\frac{I_0}{I} = K_{SV}[Q] + 1 \tag{1}$$

where $I_0$ and $I$ are the fluorescence intensities of compound **1** before and after the successive additions of $Cu^{2+}$ ions, respectively; $[Q]$ stands for quencher concentration, namely the molar concentration of the $Cu^{2+}$; and $K_{SV}$ is the Stern–Volmer quenching constant, which is an indicator of fluorescence quenching efficiency [28]. Figure 9 shows that the relative fluorescence ($I_0/I$) linearly fitted with the $Cu^{2+}$ ion concentration in the range of 1.5–5.5 μM (inset of Figure 9), while at higher concentrations, the plot shows an upward curvature, concave toward the *y*-axis. The characteristic feature of Stern–Volmer plots is indicative of a combination of static and dynamic quenching processes involving the fluorophore. In this case, the dependence of the fluorescence intensity upon quencher concentration is as follows:

$$\frac{I_0}{I} = (1 + K_D[Q]) \times (1 + K_S[Q]) \tag{2}$$

where $K_D$ and $K_S$ are the dynamic and static quenching constants, respectively [29,30]. Moreover, from this equation, from the multiplication of the terms in parentheses, it is possible to obtain the following equation:

$$K_{app} = \left[\frac{I_0}{I} - 1\right] \times \frac{1}{[Q]} = (K_D + K_S) + K_D K_S[Q] \tag{3}$$

A plot of apparent constant ($K_{app}$) versus [Q] yields a straight line with an intercept of $K_D + K_S$ and a slope of $K_S \times K_D$ (Figure 9, right). Furthermore, static and dynamic quenching can be distinguished by their different dependencies on temperature and viscosity, or preferably by lifetime measurements. We performed fluorimetric titration at three different temperatures, namely at 25, 33, and 40 °C (Supplementary Materials, Figure S1), and the results plotted in Figure 9 suggested that the change in the fluorescence intensity increases with temperature. Namely, higher temperatures yield faster diffusion, and hence larger amounts of collisional quenching occur. $K_D$ values were obtained by the slope of the regression curve in the linear range (Figure 9; Equation (1)), while $K_S$ values were estimated according to Equation (3), from the slope of the curve reported in Figure 9 (right) [30]. These results

suggest that dynamic quenching has a considerable influence on the overall quenching processes and that the increase in temperature results in a lower quenching static constant.
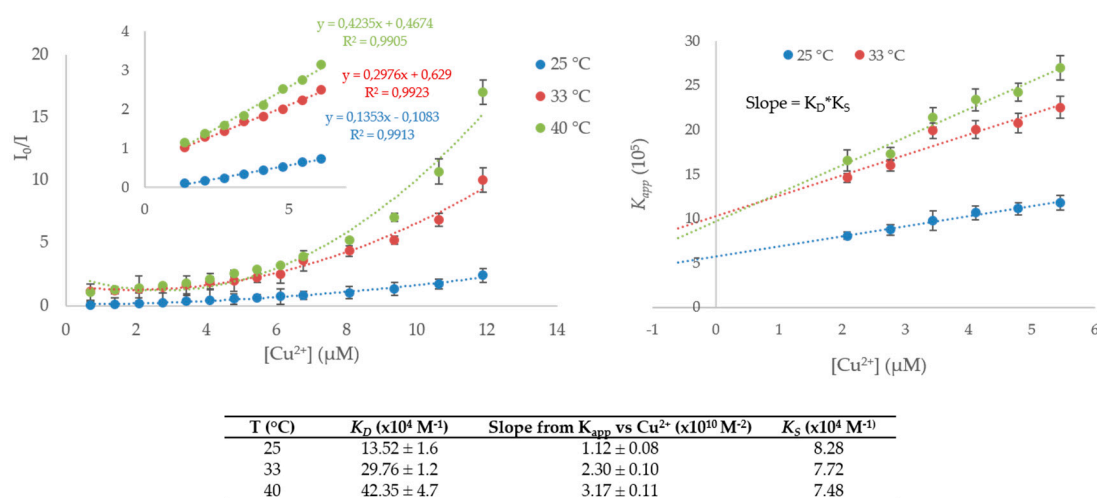


| T (°C) | $K_D$ (x10⁴ M⁻¹) | Slope from $K_{app}$ vs Cu²⁺ (x10¹⁰ M⁻²) | $K_S$ (x10⁴ M⁻¹) |
|---|---|---|---|
| 25 | $13.52 \pm 1.6$ | $1.12 \pm 0.08$ | 8.28 |
| 33 | $29.76 \pm 1.2$ | $2.30 \pm 0.10$ | 7.72 |
| 40 | $42.35 \pm 4.7$ | $3.17 \pm 0.11$ | 7.48 |

**Figure 9.** (**Left**) Stern–Volmer plots for the titration of compound **1** with $Cu^{2+}$ at different temperatures. (**Right**) Modified Stern–Volmer plots. Each experiment was performed in triplicate. The obtained quenching constants are listed in the table.

Finally, the detection limit (LOD) was calculated according to the IUPAC recommendation as LOD = $3\sigma$/slope, where $\sigma$ is the standard deviation estimated by the fluorescence intensity of the blank, and the slope is obtained from a calibration curve for the fluorescence intensity against the $Cu^{2+}$ ion concentration. Noteworthy, under these conditions, the LOD for the detection of $Cu^{2+}$ ions in the presence of compound **1** is estimated to be 0.574 μM.

The reversibility of the $Cu^{2+}$/compound **1** complex was evaluated, as shown in Figure S2 of Supplementary Materials. When the benzoxanthene **1** ($1.70 \times 10^{-5}$ M) was saturated by the addition of $Cu^{2+}$ ions (0.2 equiv.), the fluorescence intensity was approximately halved; by adding a solution of EDTA (2.0 equiv.) to the mixture, a significant increase in the fluorescence intensity (almost up to the starting fluorescence value) was observed. These results demonstrate that the $Cu^{2+}$ ion recognition of probe **1** is a reversible complexing process.

To support the experimental results, DFT calculations were performed on molecule **1** and $Cu^{2+}$/compound **1** complex. The thermal complexation energy was studied for different stoichiometries (1:1, 1:2, 1:3; $Cu^{2+}$:compound **1**). The data showed that the interaction energy ($E_{int} = E_{complex} - E_1 - E_{Cu^{2+}}$) of the 1:3 complex was favorable among the three different complexes under study, resulting in −47.582 kcal/mol. The energies of the 1:2 and 1:1 complexes were −29.707 and −14.536 kcal/mol, respectively. The results of these energy calculations are in full agreement with the titration data, supporting the formation of the 1:3 complex. The geometry of the obtained complex is shown in Figure 10. In this geometry, the copper is complexed in a tetragonally elongated octahedral complex, where two oxygen (O65 and O66) of the same molecule of compound **1** and two oxygen atoms belonging to the other two molecules (O26 and O106) are lying in the $xy$ plane, and the remaining O25 and O105 are located in the $z$-axis. The elongated octahedral is due to the Jahn–Teller effect that is often encountered in octahedral complexes of the transition metals and is very common in six-coordinate $Cu^{2+}$ complexes [31,32]. According to the crystal field theory, the complexes of copper are principally square planar, with the odd electron occupying the $dx^2$-$y^2$ orbital; any addition ligands available would take up the fifth and sixth coordination positions, but because the $dz^2$ always contains a pair of electrons, usually the fifth and sixth ligands (O25 and O105 in the case of $Cu^{2+}$/compound **1** complex) will not be able to approach the copper as closely as the ligands in the plane [33].
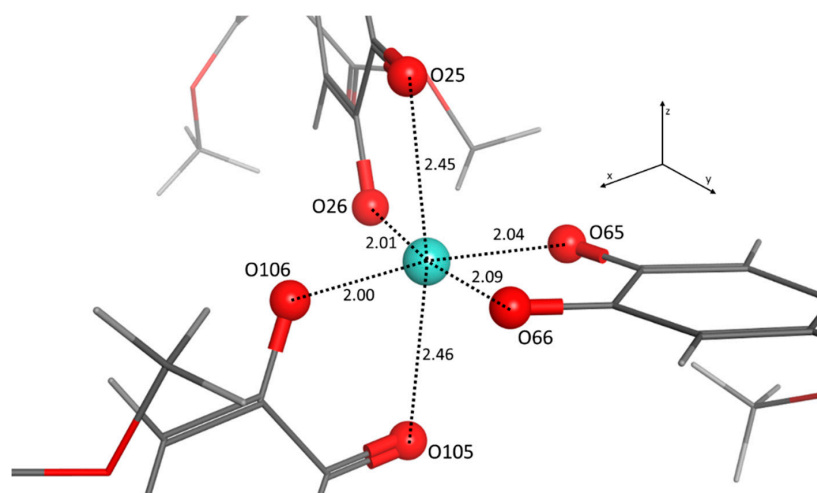
**Figure 10.** The geometry of the B3LYP/LANL2DZ optimized 1:3 $Cu^{2+}$/compound **1** complex. Bond distances are showed in angstrom.

The calculated Wiberg bond indexes for the complex are reported in Table 1, and as expected, they show the strongest interaction between the oxygen ligands in the *xy* plane and the metal. A less intense interaction is observed for the two oxygens in the *z*-axis. From the results of the secondary-order perturbation theory (SOPT) analysis of the Fock matrix in the natural bond orbital (NBO) basis, the single inter-complex contributions energies were also calculated. As expected from the obtained geometry of the complex, the strongest donor–acceptor interactions for the formation of the complex are the ones between the ion pairs of O26, O65, O66, and O106 with antibonding orbitals of the $Cu^{2+}$. The highest energy donor–acceptor interactions are reported in Table 2. The energy gap between HOMO and LUMO for molecule **1** and $Cu^{2+}$/compound **1** complex is found as 3.43 and 2.71 eV, respectively. TD-DFT calculation suggested that this transition corresponds to the first excited state. Thus, the obtained results indicate that the stabilized complex between molecule **1** and copper ion has a lower HOMO–LUMO energy gap when compared to compound **1** alone. The emission-quenching response of probe **1** was due to the strong interaction between copper and the hydroxylic groups as a result of the charge transfer process from the variation of the electronic structure of molecule **1** [34,35].

**Table 1.** Calculated Wiberg bond indexes between the indicated oxygen atoms and the $Cu^{2+}$.

| Atom | O25 | O26 | O65 | O66 | O105 | O106 |
|------|-----|-----|-----|-----|------|------|
| Wiberg bond index | 0.1263 | 0.2850 | 0.2300 | 0.2717 | 0.1283 | 0.2850 |

**Table 2.** Secondary orbital interactions for $Cu^{2+}$/compound **1** complex.

| Donor NBO | Acceptor NBO | Energy (kcal/mol) |
|-----------|--------------|-------------------|
| LP O25 | LP* Cu121 | 3.93 |
| LP O25 | LP* Cu121 | 3.81 |
| LP O26 | LP* Cu121 | 13.86 |
| LP O26 | LP* Cu121 | 12.08 |
| LP O65 | LP* Cu121 | 11.28 |
| LP O65 | LP* Cu121 | 10.14 |
| LP O66 | LP* Cu121 | 13.21 |
| LP O66 | LP* Cu121 | 9.71 |
| LP O105 | LP* Cu121 | 4.24 |
| LP O105 | LP* Cu121 | 3.89 |
| LP O106 | LP* Cu121 | 12.87 |
| LP O106 | LP* Cu121 | 12.49 |

## 3. Materials and Methods

Materials were obtained from commercial suppliers and were used without further purification. $^1$H and $^{13}$C NMR spectra of compound **1** were run on a Varian VNMR-S spectrometer (Agilent, Milan, Italy) operating at 499.86 ($^1$H) and 125.70 MHz ($^{13}$C) and equipped with a gradient-enhanced reverse detection probe. NMR spectrometry experiments were performed using software supplied by the manufacturers and acquired at constant temperature (27 °C) in $(CD_3)_2CO$.

UV-Vis measurements were performed on a JASCO V630 spectrophotometer (JASCO Europe, Cremella (LC), Italy) using 1 cm quartz cuvette at 27 °C. The spectra were acquired in the range of 200–500 nm.

Fluorescence studies of compound **1** in the presence of the selected ions were carried out in a sealed cuvette at 27 °C in a Varian Cary Eclipse spectrophotometer (Agilent, Milan, Italy). Each sample in a cell of 1 cm path length was excited at 366 nm wavelength, and the emission scans were recorded from 400 nm to 700 nm; both the slits of excitation and emission were 10 nm. For UV-Vis and fluorimetric measurements, EtOH for spectroscopy and a 20 mM phosphate buffer (pH = 7.0), freshly prepared with double distilled water, were employed.

The association constants ($K_\beta$) were determined by UV and fluorescence titrations, in conjunction with the non-linear least-square fit of the data to the models, using HypSpec software [36,37]. Several binding equilibria between compound **1** and the metals ($Ag^+$ and $Cu^{2+}$) were considered. The experimental data were either applied to single equilibrium model 1:1 or multiple binding equilibria models such as 1:1 + 1:2 + 1:3 (metals:compound **1**) models for best data fit with HypSpec software. The experimental data were tested against all the different types of binding models to establish a proper stoichiometry and association constant. The obtained values were almost identical for both UV and fluorescence titrations experiments.

### 3.1. Preparation of Methyl Ester of Caffeic Acid

Caffeic acid methyl ester was obtained by Fisher's esterification. Caffeic acid (156.5 mg, 0.87 mmol) was treated with MeOH (35 mL) in the presence of a catalytic amount of concentrated $H_2SO_4$ (0.2 mL). The resulting mixture was stirred at reflux temperature for 4 h. The mixture was diluted with ethyl acetate (100 mL), and the pure product was quantitatively recovered from the organic phase by partitioning with water.

### 3.2. Preparation of Dimethyl 6,9,10-Trihydroxybenzo[k,l]Xanthene-1,2-Dicarboxylate (**1**)

The benzoxanthene **1** was synthesized according to the previously reported biomimetic methodology. Briefly, caffeic acid methyl ester (100.2 mg, 0.26 mmol) was solubilized in $CHCl_3$ (18.5 mL), and the solution was mixed with an excess of Mn $(OAc)_3$ (278.8 mg, 1.04 mmol). The reaction mixture was stirred at room temperature for 2 h. The reaction was quenched by the addition of a saturated ascorbic acid solution (15 mL), and the mixture was partitioned. The aqueous phase was partitioned with $CH_2Cl_2$ (3 × 15 mL), the combined organic layer was dried over anhydrous $Na_2SO_4$, and the solvent was evaporated under vacuum. The residue was purified by chromatographic column on Chromabond silica diol (45 μm; Macherey-Nagel) using a gradient of MeOH in $CH_2Cl_2$ (from 1% to 5%). UV (EtOH:phosphate buffer 1:1) $\lambda_{max}$ (log $\varepsilon$) 272 (4.29), 396 (4.01) nm. $^1$H and $^{13}$C NMR data of compound **1** are in perfect agreement with those previously reported in the literature [17,21].

### 3.3. Preparation of UV-Vis and Fluorometric Titration Solutions

Stock solutions (0.01 M) of nitrate and chloride salts of $Ag^+$, $Cd^{2+}$, $Co^{2+}$, $Cu^{2+}$, $Fe^{3+}$, $Hg^{2+}$, $K^+$, $Mg^{2+}$, $Na^+$, $Ni^{2+}$, and $Zn^{2+}$ in phosphate buffer (20 mM, pH = 7.0) were prepared. A probe stock solution of compound **1** ($1.72 \times 10^{-5}$ M) was prepared using EtOH-buffer (1:1). A solution of compound **1** (3 mL) of the probe stock solution was put into a test tube and titrated with the successive addition

(10 μL) of each ion's stock solution. The spectrofluorimetric measurements were performed at 25, 33, and 40 °C, and the data were elaborated according to the Stern–Volmer equation (Equations (1)–(3)).

For competing experiments, a $1.70 \times 10^{-5}$ M solution of compound **1** was used to record fluorimetric measurements in the presence of $Cu^{2+}$ ($1.4 \times 10^{-6}$ M; control) and one of the other metals under study ($Na^+$, $K^+$, $Ag^+$, $Cd^{2+}$, $Co^{2+}$, $Hg^{2+}$, $Mg^{2+}$, $Ni^{2+}$, $Zn^{2+}$, and $Fe^{3+}$; $40 \times 10^{-6}$ M).

### 3.4. Theoretical Calculations

Molecules were drawn in Marvin Sketch (18.24, ChemAxon Ltd., Budapest, Hungary), and 3D-structures were initially generated with the Merck molecular force field (MMFF94) and then optimized at a semiempirical level using the parameterized model number 6 (PM6) Hamiltonian as implemented in the MOPAC package (MOPAC2016 v. 18.151, Stewart Computational Chemistry, Colorado Springs, CO, USA) [38], before the DFT calculations.

The DFT calculations were performed using the Gaussian 16 software (Gaussian, Inc., Wallingford, CT, USA) with B3LYP and LANL2DZ basis sets [39].

## 4. Conclusions

In conclusion, we report a benzo[*k,l*]xanthene derivative, molecule **1**, which is a selective and sensitive turn-off chemosensor that recognizes the $Cu^{2+}$ ion explicitly in an EtOH-phosphate buffer (1:1) solution by fluorescence spectroscopy. Compound **1** was selected among different previously reported compounds with a benzo[*k,l*]xanthene core, and its complexation ability toward different metal cations that are involved in biological systems or that accumulate in the environment (such as $Ag^+$, $Cd^{2+}$, $Co^{2+}$, $Cu^{2+}$, $Fe^{3+}$, $Hg^{2+}$, $K^+$, $Mg^{2+}$, $Na^+$, $Ni^{2+}$, and $Zn^{2+}$) was studied. The natural benzoxanthene **1** was shown to respond with high selectivity toward $Cu^{2+}$ over the other metal ions. Among all of the studied ions, the molecule showed an ion concentration-dependent decreasing fluorescence for $Ag^+$ and, at a lower concentration, for $Cu^{2+}$. For this latter cation, a LOD of 0.574 μM was found. The calculated $\log K_\beta$ resulted in 6.589 for $Ag^+$ and 13.265 for $Cu^{2+}$. Theoretical DFT calculation showed that the geometry of the $Cu^{2+}$/compound **1** complex is a tetragonally elongated octahedral and supported the formation of a 1:3 stoichiometry. Fluorescence experiments demonstrate that compound **1** may have application as a fluorescent probe for detecting $Cu^{2+}$ over a wide range of other cations without interferences.

**Supplementary Materials:** Supplementary Materials can be found at http://www.mdpi.com/1422-0067/21/18/6933/s1.

**Author Contributions:** Conceptualization: A.R. and C.T.; methodology: G.F. and C.S.; software: A.R.; validation: G.F. and N.C.; formal analysis: G.F. and N.C.; investigation: G.F., N.C., C.S., and A.R.; resources: A.R. and C.T.; data curation: G.F. and N.C.; writing—original draft preparation: G.F., N.C., and C.S.; writing—review and editing: G.F., N.C., A.R., and C.T.; supervision: N.C. and C.T.; project administration: A.R. and C.T.; funding acquisition: C.T. All authors have read and agreed to the published version of the manuscript.

**Conflicts of Interest:** The authors declare no conflict of interest.

## References

1. Desai, V.; Kaler, S.G. Role of copper in human neurological disorders. *Am. J. Clin. Nutr.* **2008**, *88*, 855S–858S. [CrossRef]

2. Multhaup, G.; Schlicksupp, A.; Hesse, L.; Beher, D.; Ruppert, T.; Masters, C.L.; Beyreuther, K. The amyloid precursor protein of Alzheimer's disease in the reduction of copper(II) to copper(I). *Science* **1996**, *271*, 1406–1409. [CrossRef]

3. Que, E.L.; Domaille, D.W.; Chang, C.J. Metals in neurobiology: Probing their chemistry and biology with molecular imaging. *Chem. Rev.* **2008**, *108*, 1517–1549. [CrossRef]

4.  Zong, L.Y.; Song, Y.C.; Li, Q.Q.; Li, Z. A "turn-on" fluorescence probe towards copper ions based on core-substitued naphthalene diimide. *Sens. Actuators B-Chem.* **2016**, *226*, 239–244. [CrossRef]

5.  Zhang, J.; Yu, C.W.; Qian, S.Y.; Lu, G.; Chen, J.L. A selective fluorescent chemosensor with 1,2,4-triazole as subunit for Cu (II) and its application in imaging Cu (II) in living cells. *Dyes Pigments* **2012**, *92*, 1370–1375. [CrossRef]

6.  Wang, H.H.; Xue, L.; Fang, Z.J.; Li, G.P.; Jiang, H. A colorimetric and fluorescent chemosensor for copper ions in aqueous media and its application in living cells. *New J. Chem.* **2010**, *34*, 1239–1242. [CrossRef]

7.  Lu, D.L.; Lei, J.Y.; Tian, Z.D.; Wang, L.Z.; Zhang, J.L. Cu2+ fluorescent sensor based on mesoporous silica nanosphere. *Dyes Pigments* **2012**, *94*, 239–246. [CrossRef]

8.  Meng, Q.T.; Shi, Y.; Wang, C.P.; Jia, H.M.; Gao, X.; Zhang, R.; Wang, Y.F.; Zhang, Z.Q. NBD-based fluorescent chemosensor for the selective quantification of copper and sulfide in an aqueous solution and living cells. *Org. Biomol. Chem.* **2015**, *13*, 2918–2926. [CrossRef]

9.  Daquino, C.; Rescifina, A.; Spatafora, C.; Tringali, C. Biomimetic synthesis of natural and "unnatural" lignans by oxidative coupling of caffeic esters. *Eur. J. Org. Chem.* **2009**, *2009*, 6289–6300. [CrossRef]

10. Bhusainahalli, V.M.; Spatafora, C.; Chalal, M.; Vervandier-Fasseur, D.; Meunier, P.; Latruffe, N.; Tringali, C. Resveratrol-related dehydrodimers: Laccase-mediated biomimetic synthesis and antiproliferative activity. *Eur. J. Org. Chem.* **2012**, *2012*, 5217–5224. [CrossRef]

11. Cardullo, N.; Pulvirenti, L.; Spatafora, C.; Musso, N.; Barresi, V.; Condorelli, D.F.; Tringalii, C. Dihydrobenzofuran neolignanamides: Lactase-mediated biomimetic synthesis and antiproliferative activity. *J. Nat. Prod.* **2016**, *79*, 2122–2134. [CrossRef]

12. Di Micco, S.; Spatafora, C.; Cardullo, N.; Riccio, R.; Fischer, K.; Pergola, C.; Koeberle, A.; Werz, O.; Chalal, M.; Vervandier-Fasseur, D.; et al. 2,3-Dihydrobenzofuran privileged structures as new bioinspired lead compounds for the design of mPGES-1 inhibitors. *Bioorg. Med. Chem.* **2016**, *24*, 820–826. [CrossRef]

13. Pulvirenti, L.; Muccilli, V.; Cardullo, N.; Spatafora, C.; Tringali, C. Chemoenzymatic synthesis and alpha-glucosidase inhibitory activity of dimeric neolignans inspired by magnolol. *J. Nat. Prod.* **2017**, *80*, 1648–1657. [CrossRef]

14. Baschieri, A.; Pulvirenti, L.; Muccilli, V.; Amorati, R.; Tringali, C. Chain-breaking antioxidant activity of hydroxylated and methoxylated magnolol derivatives: The role of H-bonds. *Org. Biomol. Chem.* **2017**, *15*, 6177–6184. [CrossRef]

15. Di Micco, S.; Pulvirenti, L.; Bruno, I.; Terracciano, S.; Russo, A.; Vaccaro, M.C.; Ruggiero, D.; Muccilli, V.; Cardullo, N.; Tringali, C.; et al. Identification by Inverse Virtual Screening of magnolol-based scaffold as new tankyrase-2 inhibitors. *Bioorg. Med. Chem.* **2018**, *26*, 3953–3957. [CrossRef]

16. Cardullo, N.; Barresi, V.; Muccilli, V.; Spampinato, G.; D'Amico, M.; Condorelli, D.F.; Tringali, C. Synthesis of bisphenol neolignans inspired by honokiol as antiproliferative agents. *Molecules* **2020**, *25*, 733. [CrossRef]

17. Spatafora, C.; Barresi, V.; Bhusainahalli, V.M.; Di Micco, S.; Musso, N.; Riccio, R.; Bifulco, G.; Condorelli, D.; Tringali, C. Bio-inspired benzo[*k,l*]xanthene lignans: Synthesis, DNA-interaction and antiproliferative properties. *Org. Biomol. Chem.* **2014**, *12*, 2686–2701. [CrossRef]

18. Qu, Z.Y.; Zhang, Y.W.; Yao, C.L.; Jin, Y.P.; Zheng, P.H.; Sun, C.H.; Liu, J.X.; Wang, Y.S.; Wang, Y.P. Chemical constituents from Orobanche cernua Loefling. *Biochem. Syst. Ecol.* **2015**, *60*, 199–203. [CrossRef]

19. Genovese, C.; Pulvirenti, L.; Cardullo, N.; Muccilli, V.; Tempera, G.; Nicolosi, D.; Tringali, C. Bioinspired benzoxanthene lignans as a new class of antimycotic agents: Synthesis and Candida spp. growth inhibition. *Nat. Prod. Res.* **2020**, *34*, 1653–1662. [CrossRef]

20. Gerstmeier, J.; Kretzer, C.; Di Micco, S.; Miek, L.; Butschek, H.; Cantone, V.; Bilancia, R.; Rizza, R.; Troisi, F.; Cardullo, N.; et al. Novel benzoxanthene lignans that favorably modulate lipid mediator biosynthesis: A promising pharmacological strategy for anti-inflammatory therapy. *Biochem. Pharmacol.* **2019**, *165*, 263–274. [CrossRef]

21. Di Micco, S.; Mazue, F.; Daquino, C.; Spatafora, C.; Delmas, D.; Latruffe, N.; Tringali, C.; Riccio, R.; Bifulco, G. Structural basis for the potential antitumour activity of DNA-interacting benzo[kl]xanthene lignans. *Org. Biomol. Chem.* **2011**, *9*, 701–710. [CrossRef]

22. Spatafora, C.; Daquino, C.; Tringali, C.; Amorati, R. Reaction of benzoxanthene lignans with peroxyl radicals in polar and non-polar media: Cooperative behaviour of OH groups. *Org. Biomol. Chem.* **2013**, *11*, 4291–4294. [CrossRef]

23. Capolupo, A.; Tosco, A.; Mozzicafreddo, M.; Tringali, C.; Cardullo, N.; Monti, M.C.; Casapullo, A. Proteasome as a new target for bio-inspired benzo[*k,l*]xanthene lignans. *Chem. Eur. J.* **2017**, *23*, 8371–8374. [CrossRef]

24. Truter, M.R. Recognition of metal cations by biological systems. *Philos. Trans. R. Soc. B Biol. Sci.* **1975**, *272*, 29–41.

25. De Courcy, B.; Pedersen, L.G.; Parisel, O.; Gresh, N.; Silvi, B.; Pilme, J.; Piquemal, J.P. Understanding selectivity of hard and soft metal cations within biological systems using the subvalence concept. I. Application to blood coagulation: Direct cation-protein electronic effects vs. indirect interactions through water networks. *J. Chem. Theory Comput.* **2010**, *6*, 1048–1063. [CrossRef]

26. Fabbrizzi, L.; Licchelli, M.; Pallavicini, P.; Sacchi, D.; Taglietti, A. Sensing of transition metals through fluorescence quenching or enhancement—A review. *Analyst* **1996**, *121*, 1763–1768. [CrossRef]

27. Li, L.N.; Shen, S.S.; Lin, R.Y.; Bai, Y.; Liu, H.W. Rapid and specific luminescence sensing of Cu(II) ions with a porphyrinic metal-organic framework. *Chem. Commun.* **2017**, *53*, 9986–9989. [CrossRef]

28. Cardullo, N.; Muccilli, V.; Pulvirenti, L.; Cornu, A.; Pouysegu, L.; Deffieux, D.; Quideau, S.; Tringali, C. C-glucosidic ellagitannins and galloylated glucoses as potential functional food ingredients with anti-diabetic properties: A study of alpha-glucosidase and alpha-amylase inhibition. *Food Chem.* **2020**, *313*, 126099. [CrossRef]

29. Lakowicz, J.R. Quenching of fluorescence. In *Principles of Fluorescence Spectroscopy*; Lakowicz, J.R., Ed.; Springer: Boston, MA, USA, 2006; pp. 277–328.

30. Ghosh, K.S.; Sahoo, B.K.; Jana, D.; Dasgupta, S. Studies on the interaction of copper complexes of (-)-epicatechin gallate and (-)-epigallocatechin gallate with calf thymus DNA. *J. Inorg. Biochem.* **2008**, *102*, 1711–1718. [CrossRef]

31. Liao, Q.; Kamerlin, S.C.; Strodel, B. Development and application of a nonbonded Cu(2+) model that Includes the Jahn-Teller effect. *J. Phys. Chem. Lett.* **2015**, *6*, 2657–2662. [CrossRef]

32. Hosain, M.A.; Le Floch, J.M.; Krupka, J.; Tobar, M.E. Aggregate frequency width, nuclear hyperfine coupling and Jahn-Teller effect of Cu(2+) impurity ion ESR in SrLaAlO4 dielectric resonator at 20 millikelvin. *J. Phys. Condens. Matter* **2018**, *30*, 015802. [CrossRef] [PubMed]

33. Manch, W.; Fernelius, W.C. The structure and spectra of nickel(II) and copper(II) complexes. *J. Chem. Educ.* **1961**, *38*, 192. [CrossRef]

34. Hwang, S.M.; Chae, J.B.; Kim, C. A phenanthroimidazole-based fluorescent turn-off chemosensor for the selective detection of Cu2+ in aqueous media. *Bull. Korean Chem. Soc.* **2018**, *39*, 925–930. [CrossRef]

35. Arslan, F.N.; Geyik, G.A.; Koran, K.; Ozen, F.; Aydin, D.; Elmas, S.N.K.; Gorgulu, A.O.; Yilmaz, I. Fluorescence "turn on-off" sensing of copper (II) ions utilizing coumarin-based chemosensor: Experimental study, theoretical calculation, mineral and drinking water analysis. *J. Fluoresc.* **2020**, *30*, 317–327. [CrossRef]

36. Cox, R.M.; Rivera, I.M. Predictability and reliability of hearing aid benefit measured using the PHAB. *J. Am. Acad. Audiol.* **1992**, *3*, 242–254.

37. Gans, P.; Sabatini, A.; Vacca, A. Investigation of equilibria in solution. Determination of equilibrium constants with the HYPERQUAD suite of programs. *Talanta* **1996**, *43*, 1739–1753. [CrossRef]

38. Stewart, J.J.P. Optimization of parameters for semiempirical methods IV: Extension of MNDO, AM1, and PM3 to more main group elements. *J. Mol. Model.* **2004**, *10*, 155–164. [CrossRef]

39. Frisch, M.J.; Trucks, G.W.; Schlegel, H.B.; Scuseria, G.E.; Robb, M.A.; Cheeseman, J.R.; Scalmani, G.; Barone, V.; Petersson, G.A.; Nakatsuji, H.; et al. *Gaussian 16 Rev. C.01*; Gaussian, Inc.: Wallingford, CT, USA, 2016.